Structure and dynamics of a lipid nanodisc by integrating NMR, SAXS and SANS experiments with molecular dynamics simulations

Tone Bengtsen,[†] Viktor L. Holm,[‡] Søren R. Midtgaard,[‡] Nicolai Tidemand Johansen,[‡] Sandro Bottaro,[†] Lise Arleth,[*,‡] and Kresten Lindorff-Larsen[*,†]

[†]*Structural Biology and NMR Laboratory & Linderstrøm-Lang Centre for Protein Science, Department of Biology, University of Copenhagen. Ole Maaløes Vej 5, DK-2200 Copenhagen, Denmark*

[‡]*Structural Biophysics, X-ray and Neutron Science, Niels Bohr Institute, University of Copenhagen, DK-2100 Copenhagen, Denmark*

E-mail: arleth@nbi.ku.dk; lindorff@bio.ku.dk

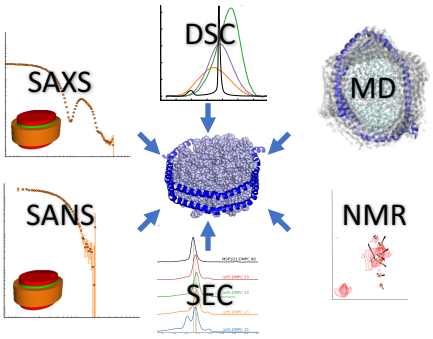

Abstract

Nanodiscs are membrane mimetics that consist of a protein belt surrounding a small lipid bilayer. Nanodiscs are of broad use for solution-based characterization of membrane proteins, but we still lack a full understanding of their structure and dynamics. Recently, NMR and EPR experiments provided a view of the average structure of the nanodisc's protein component, and small-angle X-ray and neutron scattering experiments have provided insight into the global structural properties of both protein and lipids. Here, we investigate the structure, dynamics and biophysical properties of two small nanodiscs, MSP1D1ΔH5 and ΔH4H5. We use differential scanning calorimetry to compare the melting transition of DMPC in nanodiscs of different sizes with DMPC vesicles, and find that the ordering of the lipids is highly dependent on the nanodisc size. Using combined SEC-SAXS and SEC-SANS experiments, we obtain low-resolution structures of the nanodiscs and find that these have the shape of elliptical discs. These structures are in apparent contrast to the NMR/EPR structure, which showed a more circular conformation. We reconcile these views by using a Bayesian/Maximum Entropy method to combine molecular dynamics simulations of MSP1D1ΔH5 with the NMR and SAXS experiments. We derive a conformational ensemble representing the structure and dynamics of the nanodisc, and find that it displays conformational heterogeneity with various elliptical shapes that explain both the SAXS and NMR data. Together, our results demonstrate the power of integrative modelling and paves the way for future studies of larger complex systems such as membrane proteins embedded in nanodiscs.

Introduction

Nanodiscs are widely used membrane models that facilitate biophysical studies of membrane proteins.[1] They are derived from, and very similar to, the human ApoA1 protein from high density lipoproteins (HDL particles) and consists of two amphipatic membrane scaffold proteins (MSP's) that stack and encircle a small patch of lipids in a membrane bilayer to form a discoidal assembly. The popularity of nanodiscs arises from their ability to mimic a membrane while at the same time ensuring a small system of homogeneous composition whose size can be controlled and can give diameters in a range from about 7 to 13 nm.[2,3]

Despite the importance of nanodiscs in structural biology research and the medical importance of HDL particles, we still lack detailed structural models of these protein-lipid particles. The nanodisc has so far failed to crystallize, so in order to study its structure and dynamics a range of biophysical methods have been used to provide information about specific characteristics. For example, mass spectrometry experiments have provided insight into lipid-water interactions and heterogeneous lipid compositions,[4,5] and small angle X-ray scattering (SAXS) and -neutron scattering (SANS) have provided insight into the size and low resolution shape of nanodiscs in solution.[2,6–8] These experiments have been complemented by molecular dynamics (MD) simulations that provided both pioneering insights into the structure[9,10] as well as a better understanding of the assembly process, lipid-protein interactions and membrane mimicking effects.[11–13]

Recently, the first high resolution experimental structure of the MSP protein belt encircling the nanodisc was obtained from the small, helix-5-deleted nanodisc, MSP1D1ΔH5 (henceforth ΔH5), reconstituted with DMPC lipids (ΔH5-DMPC).[14] The structure provided an important step towards a better understanding of the nanodisc and was obtained by combining nuclear magnetic resonance (NMR) spectroscopy, electron paramagnetic resonance (EPR) spectroscopy and transmission electron microscopy (TEM).[14] While these experiments were performed on lipid-loaded nanodiscs, the study focused on the protein components, and on determining a time- and ensemble averaged structure of these, but left

open the question of the role of the lipids as well as any structural dynamics of the overall nanodisc.[15] Intriguingly, the resulting structure of the belt proteins corresponded to that of an almost circularly-shaped disc, while our previous SAXS/SANS investigations are clearly consistent with discs with an on-average elliptical cross-section.[6,8]

Here we continue the quest to understand the structure and dynamics of the nanodisc. We performed SAXS and SANS experiments on the ΔH5-DMPC variant, and integrated these with MD simulations and previously published NMR data[14] through an integrative Bayesian/maximum entropy (BME) approach.[16–19] We thereby obtain a model of the conformational ensemble of the ΔH5-DMPC nanodisc that is consistent with the structural information obtained from each method, as well as our molecular simulations, and successfully explains differences in previous structural interpretations. In addition, our Differential Scanning Calorimetry (DSC) measurements of the melting transition of DMPC in differently sized nanodiscs provides information about the internal dynamics of the encircled lipid bilayer. This study shows how multiple methods and their integration helps simultaneously understand the structure and the dynamics of a complex protein-lipid system, and paves the way for future studies of complex biophysical systems such as membrane proteins.

Results and Discussion

Reconstitution of ΔH5-DMPC and ΔH4H5-DMPC nanodiscs

We determined optimal reconstitution ratios between the DMPC lipids and the ΔH5 and ΔH4H5 protein belts to form lipid-saturated nanodiscs through a size-exclusion chromatography (SEC) analysis (Fig. S1). We found that reconstitution ratios of 1:33 for ΔH4H5:DMPC and 1:50 for ΔH5:DMPC were optimal in order to form single and relatively narrow symmetric peaks. In comparison, Hagn et al.[3] previously reported ratios of 1:20 for ΔH4H5:DMPC and 1:50 for ΔH5:DMPC. As expected, more narrow and well-defined SEC-peaks were obtained if the reconstitution took place at or above the melting temperature, T_M, of DMPC

at 24 °C. In this initial analysis we investigated nanodiscs with both POPC and DMPC lipids, as these two lipids are known to behave similarly in combination with the standard MSP1D1 belt, but with slightly different optimal reconstitution ratios due to different lipid areas per headgroup.[20] In the cases of ΔH5 and ΔH4H5 we, however, found that neither of these smaller belt proteins had well-defined optimal MSP:lipid ratios when reconstituted with POPC, suggesting a lower intrinsic stability of these smaller nanodisc-types compared to the standard size MSP1D1 nanodisc.

DSC analysis of lipid melting in nanodiscs

We proceeded to study and compare the membrane mimicking ability of the nanodiscs using DSC to study the lipid melting transition of DMPC in ΔH4H5 and ΔH5 in comparison with the larger MSP1D1 nanodiscs and pure DMPC vesicles. Our results show that the melting transition peak broadens significantly in all three nanodisc systems compared to that of pure DMPC vesicles (Fig. 1), and that the transition enthalpy per mole of DMPC, i.e. the area under the curves, increases with the nanodisc size. This broadening and the size-dependent increase of the transition enthalphy are consistent with previous observations for, respectively, DMPC and DPPC in MSP1D1 and in the larger MSP1E3D1 systems.[21] Since the lipid area-to-rim ratio increases with increasing nanodisc size, Denisov *et al.* proposed that these observations were simply due to the absence of a cooperative melting transition of the lipids at the nanodisc rim.[21]

Interestingly, we observe that the maximum of the melting transition, T_M, depends on the choice of nanodisc belt and can fall both below and above the T_M of plain DMPC vesicles which we measure to 24 °C. In the smallest ΔH4H5 nanodisc, the DMPC has a $T_M \approx 22.5$ °C. In ΔH5 the DMPC has T_M at 24.5 °C which is close to that of the DMPC vesicles, while the larger MSP1D1 nanodisc has a $T_M \approx 28$ °C. This T_M value is similar to the value of 28.5 °C measured for DMPC melting in MSP1D1 by Denisov *et al.*,[21] who in addition measured a T_M value of 27.5 °C in the even larger MSP1E3D1 discs.

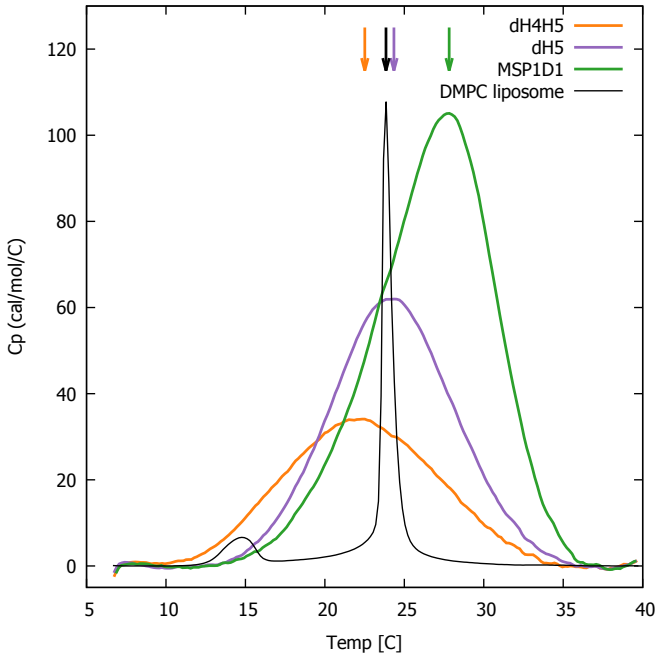

Figure 1: ***DSC analysis of lipid melting in nanodiscs***. *The three DMPC-filled nanodiscs studied, listed by increasing size, are ΔH4H5-DMPC (orange), ΔH5-DMPC (purple) and MSP1D1-DMPC (green). DSC data from plain DMPC-vesicles (black) are plotted for comparison. Arrows indicates the temperature with maximal heat capacity. DSC data from the three nanodisc samples are normalized by DMPC concentration, while the data from the DMPC liposome is on arbitrary scale.*

Our new measurements, together with those from Denisov *et al.*, show that the T_M of the DMPC can both be lowered for the small ΔH4H5 belts and increased for the MSP1D1 and MSP1E3D1, and point towards a non-trivial effect of the DMPC-MSP interactions which can apparently both destabilize DMPC in the gel-phase leading to the lower T_M compared to the DMPC vesicles (as we observe in the case of ΔH4H5-DMPC), but also stabilize the DMPC gel-phase (as observed through the higher T_M measured in the cases of MSP1D1-DMPC and MSP1E3D1-DMPC). For all three discs, we note that the melting starts already at around 10 °C below the T_M and that the transition does not start leveling off to a plateau until at around 10 °C above the T_M. Furthermore, the pre-transition visible at 15 °C for the DMPC vesicles, is not visible in any of the nanodisc systems. Together these results suggest that the state of the ordering of the lipids is more inhomogeneous in the nanodiscs compared to the DMPC vesicle and that the behaviour of the lipids is modulated by their interaction with the membrane scaffold proteins as has also been shown by NMR.[15] It remains to be studied how such perturbations relate to perturbations in the context of the high protein concentration in biological membranes.

Structural investigations by SAXS and SANS

We studied the shape of ΔH5 and ΔH4H5 nanodiscs with DMPC through combined SEC-SAXS and SEC-SANS experiments (Fig. 2). Both experiments were performed at 10 °C due to constraints of the experimental setup and the DMPC bilayer is therefore expected to be in the gel-phase based on the above presented DSC analysis. Our SAXS and SANS data all exhibit a flat Guinier region at low q and indicate no signs of aggregation (Fig. 2A, B). In both the ΔH5-DMPC and ΔH4H5-DMPC systems, the SAXS data exhibit an oscillation at medium to high q ([0.05:0.2] Å^{-1}) arising from the negative excess scattering length density of the hydrophobic alkyl-chain bilayer core and the positive excess scattering length density of the hydrophilic lipid PC-headgroups and the amphipathic protein belt. The SANS data decreases monotonically as a function of q in accordance with the homogeneous contrast

situation present here. These two different contrast situations, core-shell-contrast for SAXS and bulk-contrast for SANS, are also clearly reflected in the obtained $p(r)$-functions (Fig. 2C, D), which also confirm that the ΔH5-DMPC nanodiscs are slightly larger than the ΔH4H5-DMPC nanodiscs. The data are in qualitative agreement with the SAXS and SANS data obtained for MSP1D1 nanodiscs[2,6] and similar systems,[7,8] and indicates a discoidal structure.

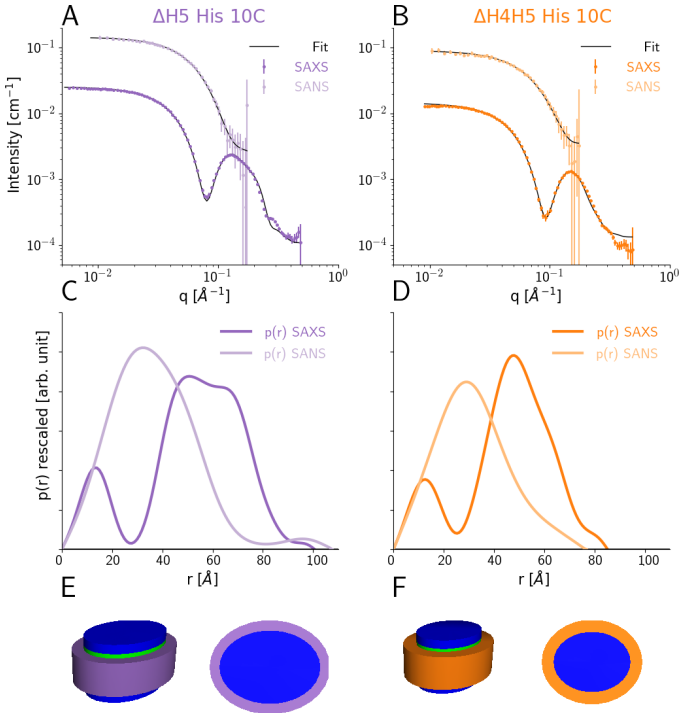

Figure 2: ***SEC-SAXS and SEC-SANS analysis of nanodiscs.*** ***A)*** *SEC-SAXS (dark purple) and SEC-SANS (light purple) for ΔH5-DMPC nanodiscs at 10 °C. The continuous curve show the model fit corresponding to the geometric nanodisc model shown in E.* ***B)*** *SEC-SAXS (dark orange) and SEC-SANS (light orange) data for the ΔH4H5-DMPC nanodiscs at 10 °C.* ***C,D)*** *Corresponding pair-distance distribution functions.* ***E, F)*** *Fitted geometrical models for the respective nanodiscs (drawn to scale relative to one another).*

We analyzed the SEC-SAXS and -SANS data simultaneously by global fitting of a previously developed molecular-constrained geometrical model for the nanodiscs[6,22] using the WillItFit Software developed in our laboratory.[23] The nanodisc model (see further details in methods section) describes the interior of the nanodisc as a stack of flat, elliptically-shaped bilayer discs to account for the hydrophobic bilayer that is sandwiched in between the two

hydrophilic headgroup layers. The inner lipid nanodisc is encircled by a hollow cylinder with an elliptical cross-section, which models the two protein MSP-belts stacked upon one another (Fig. 2E, F). Using this model, we obtained excellent simultaneous fits to SAXS and SANS data for both the ΔH4H5-DMPC and ΔH5-DMPC nanodiscs (Fig. 2A, B).

From the fitted parameters (Table 1 left) we found the area per headgroup for DMPC for both systems to be close to 55 Å^2. This value is somewhat higher than the A_{head} of gel-phase DMPC which is reported to be 47.2±0.5 Å^2 at 10 °C.[24] Our finding of larger average A_{head}-values in the ΔH4H5 and ΔH5 nanodiscs is in agreement with the very broad melting transition observed in our DSC data. The fitting revealed that the number of DMPC molecules in the nanodiscs were 65±13 and 100±14 for ΔH4H5 and ΔH5, respectively. These values are in good agreement with the optimal reconstitution ratios reported above. We note that both the SAXS and SANS data had to be re-scaled by a constant close to unity to fit the data (Table 1). In the case of the ΔH4H5-DMPC SANS data, the scaling constant (1.7±0.5) was larger than expected which is most likely the result of a less accurate protein concentration determination for this system. In addition to the structural parameters reported, small constant corrections to the background were fitted to the SAXS and SANS data. Both the ΔH4H5 and ΔH5 proteins have protruding His_6-tags linked to them via a TEV cleavage site, these 23 amino acids were assumed to be disordered and included in the model as a Gaussian random coil of R_G=12.7 Å as estimated from previous studies of disordered proteins.[25] Also an interface-roughness of nanodiscs of 2 Å were included in the model. Both the His-tag and roughness inclusion are in accordance with our previously developed methodology.[6,22,23] We note that the fitted parameters of the geometric models suggest that both nanodiscs were found to be slightly elliptical, with ratios of the two axes between 1.2 and 1.4. This observation is in apparent contrast to the recently described integrative NMR/EPR structural model of the ΔH5-DMPC nanodisc which was found to be more circular.[14]

Table 1: ***Parameters of the SAXS and SANS model fit. Left)*** *Parameters for the simultaneous model fits to SEC-SAXS and SEC-SANS of His-tagged nanodiscs (denoted -His) for both ΔH4H5-DMPC and ΔH5-DMPC. Both measurements were obtained at 10 °C.* ***Right)*** *Standard solution SAXS measurements of the ΔH5-DMPC nanodisc without His-tags (denoted -ΔHis) obtained at two different temperatures, in the gel phase at 10 °C and in the liquid phase at 30 °C. * marks parameters kept constant.*

	SEC-SAXS+SEC-SANS		**SAXS**	
	ΔH4H5-His	**ΔH5-His**	**ΔH5-ΔHis**	**ΔH5-ΔHis**
T	10 ^{o}C	10 ^{o}C	10 ^{o}C	30 ^{o}C
$\chi^2_{reduced}$	1.95	5.12	3.76	2.40
	Fitting Parameters			
Axis Ratio	1.3±0.4	1.2±0.2	1.4±0.1	1.3±0.1
A_{Head}	55± 5 Å^2	54± 2 Å^2	52± 2 Å^2	60± 3
H_{Belt}	24* Å^2	24* Å^2	24* Å^2	24* Å^2
N_{Lipid}	65±13	100±14	102± 7	104± 9
CV_{belt}	1*	1*	1*	0.97±0.02
CV_{lipid}	1.00±0.02	1.01±0.01	1.003±0.007	1.044±0.007
Scale$_{x-ray}$	1.13±0.28	1.1±0.2	1.2±0.1	1.2±0.2
Scale$_{neutron}$	1.7±0.5	0.8±0.2	-	-
	Results From Fits			
H_{lipid}	40 Å	41 Å	41 Å	38 Å
H_{tails}	28 Å	28 Å	29 Å	26 Å
R_{major}	27 Å	32 Å	34 Å	36 Å
R_{minor}	21 Å	27 Å	25 Å	28 Å
W_{belt}	10 Å	9 Å	9 Å	9 Å

Temperature dependence probed by SAXS and SANS

We continued to investigate the impact of temperature and the presence of the His-tags on both the SAXS measurements and the resulting geometrical model of ΔH5-DMPC. To do so, we acquired standard solution SAXS data for a new preparation of the ΔH5-DMPC nanodiscs, this time without His-tags and measured at both 10 °C and 30 °C. At these two temperatures the DMPC is expected to be dominantly in the gel and liquid phase, respectively, as they are below and above the melting transition temperature (Fig. 1). We used a standard solution SAXS setup for these measurements, as this at present provides a better control of both the sample temperature and sample concentration than in the SEC-SAXS based measurement. The effect of the DMPC melting transition is clearly reflected

in the SAXS data (Fig. S2) where both the position of the first minimum and the shape of the oscillation changes as the DMPC transitions from the gel to the molten state. In addition, we note that the intensity of the forward scattering decreases significantly with increasing temperature. This is a result of the small but significant temperature-dependent change of the partial specific molecular volume of the DMPC and hence a change in its excess scattering length density. To analyze the data, we again applied the molecular constrained geometrical model for the nanodiscs (Table 1, Right). Here, the effect of the DMPC melting transition can clearly be seen on the obtained DMPC area per headgroup which increases significantly as a result of the melting. Qualitatively similar observations of the melting transition of DMPC and DPPC based nanodiscs were previously reported in the MSP1D1 and MSP1E3D1 nanodiscs using DSC, SAXS and fluorescence.[21,26]

As a final control, we used the standard solution SAXS experiments to verify that the above use of His-tags in the SEC-SAXS and SEC-SANS measurements did not affect the overall structural properties. These data and the corresponding model fits show that, as expected, a similar nanodisc structure is obtained with and without His-tags (Fig. S2), and confirm the model derived from the corresponding His-tagged versions of the ΔH5-DMPC, with an overall elliptical shape (axis ratio 1.3 ±0.1).

To summarize our experimental results, we find that the melting transition of DMPC lipids in nanodiscs is much broader than in vesicles. A comparison of the nanodisc melting behaviour as a function of nanodisc size, suggests that the lipids near the protein rim must be perturbed. As a result, the melting transition temperatures for the differently sized nanodiscs are shifted as compared to that of DMPC in vesicles. Our combined SAXS and SANS analysis of both ΔH4H5-DMPC and ΔH5-DMPC nanodiscs show that both are structurally well described by an adaptation of our previously proposed model for discoidal nanodiscs.[6,22,23] We find that the axis ratio of the disc cross-section lies in the range of 1.2 to 1.4 for both sizes of nanodiscs, when interpreted by coarse-grained, single-conformation models.

Molecular Dynamics Simulations

The results described above suggest an apparent discrepancy of the solution structure of the ΔH5-DMPC nanodisc when viewed either by NMR/EPR or SAXS/SANS. In particular, the NMR/EPR structure revealed a rounded shape whereas the SAXS/SANS experiments suggested an elliptical shape. The two kinds of experiments, however, differ substantially in the aspects of the structure that they are sensitive to. Further, both sets of models were derived in a way to represent the distribution of conformations in the experiments by a single 'average' structure.

In order to understand the structural discrepancies between the two solution methods better, and to include effects of multi-conformational averaging, we proceeded by investigating the underlying structural dynamics at a detailed atomistic level through a set of MD simulations of the His-tag truncated ΔH5-DMPC nanodisc. In these simulations, we mimicked the experimental conditions of the standard solution SAXS measurements obtained at 30°C and used 100 DMPC lipids in the bilayer as found above. We performed two simulations (total simulation time of 1196 ns) using the CHARMM36m force field.[27] We visualized the conformational ensemble of the ΔH5-DMPC nanodisc by clustering the simulations, and found that the three most populated clusters represent 95% of the simulations. Notably, these structures all have elliptical shapes, but differ in the directions of the major axis (Fig. 3A).

We then examined the extent to which the simulations agree with the ensemble-averaged experimental data, focusing on the SAXS experiments and NOE-derived distance information from NMR. We calculated the SAXS intensities from the simulation frames using both FOXS[28,29] (Fig. 3B) and CRYSOL[30] (Fig. S3) and compared to the corresponding standard solution SAXS experiments obtained at 30 °C. Similarly, we used r^{-3}-weighted averaging to calculate the effective distances in the simulations and compared them to the previously reported methyl (Fig. 3C) and amide NOEs (Fig. S4).[14] The discrepancy observed between the simulation and the experiments were quantified by calculating χ^2 (Table 2).

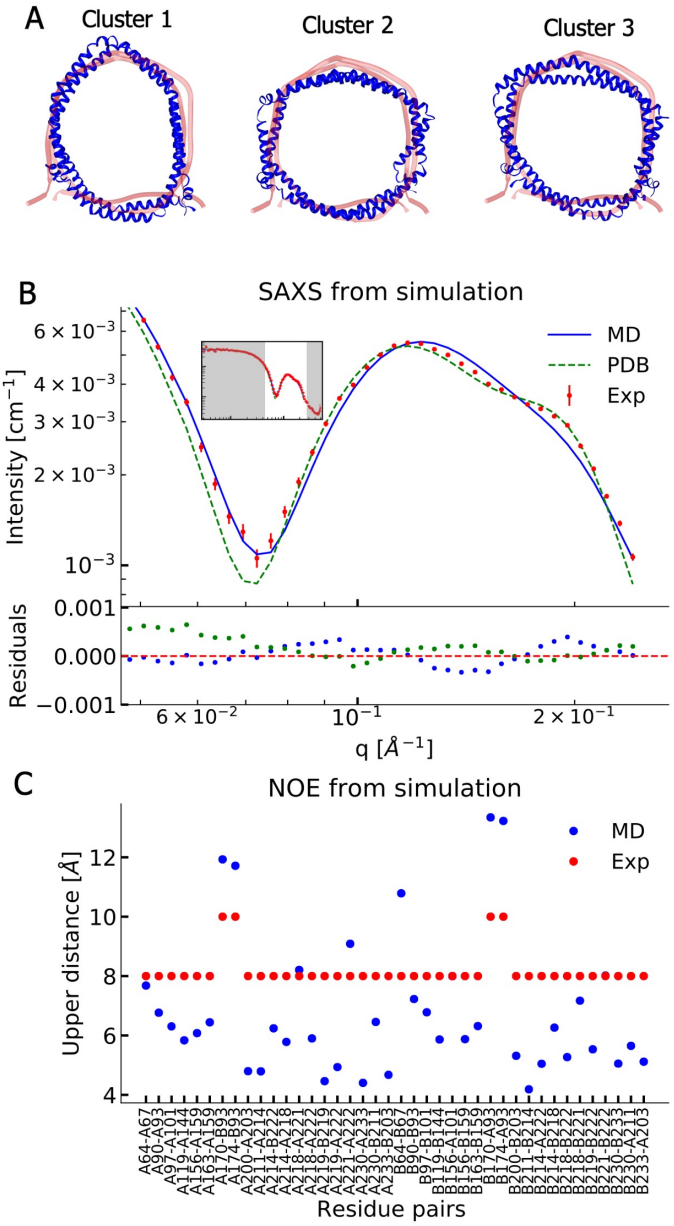

Figure 3: ***Comparing MD simulations with experiments.*** ***A)*** *Visualization of the conformational ensemble from the MD simulation by clustering (blue). Only the protein parts of the nanodisc are visualized while the lipids are left out to emphasize the shape. The top three clusters contain 95% of all frames. The previous NMR/EPR-structure is shown for comparison (red).* ***B)*** *Comparison of experimental standard solution SAXS data (red) and SAXS calculated from the simulation (blue). Green dotted line is the back-calculated SAXS from the integrative NMR/EPR-structure (labelled PDB). Residuals for the calculated SAXS curves are shown below. Only the high q-range is shown as the discrepancy between simulation and experiments are mainly located here, for the entire q-range see Fig. S3.* ***C)*** *Comparison of average distances from simulations (blue) to upper-bound distance measurements (red) between methyl NOEs. The labels show the residues which the atoms of the NOEs belong to.*

Table 2: ***Comparing experiments and simulations*** *We quantify agreement between SAXS and NMR NOE experiments by calculating the χ^2. The previously determined NMR structure[14] (PDB ID 2N5E) is labelled PDB, the unbiased MD simulation by MD, and simulations reweighted by experiments are labelled by MD and the experiments used in reweighting. S_{rel} is a measure of the amount of reweighting used to fit the data[18] (see Methods for more details).*

Data for integration	S_{rel}	χ^2	
		SAXS	NOE
PDB	–	2.9	9.5
MD	0	10.0	8.2
MD + SAXS	-1.7	1.5	7.9
MD + NOE	-1.9	8.9	4.2
MD + SAXS + NOE	-1.7	1.9	6.0

The comparison between experiments and simulations reveal an overall good agreement between the two. Interestingly, the simulations agree well with the SAXS data in the q-region where scattering is dominated by the lipid bilayer and where our geometric fitting of the models for SAXS generally are very sensitive. The MD simulation trajectory captures accurately the depth of the SAXS minimum around $q = 0.07$; however, the shoulder observed in the experiments in the range 0.15 Å^{-1} – 0.20 Å^{-1} is not captured accurately.

Direct comparison of the previously determined integrative NMR/EPR structure[14] to the SAXS data is made difficult by the missing lipids in the structure. We thus built a model of the lipidated structure by first adding DMPC lipids to the NMR/EPR solved structure (PDB ID 2N5E), and then equilibrating only the lipids by MD, keeping the protein conformation fixed. When we use this structure to calculate the SAXS data, the back-calculated data overshoots the depth of the SAXS minimum but captures well the shoulder observed in the experimental data (Fig. 3B). Thus, neither the MD trajectory nor the NMR/EPR structure fit perfectly with the measured SAXS data.

When comparing the simulations to the NMR-derived distances between methyl groups (Fig. 3C), we generally find good agreement, but observe a few distances that exceed the experimental upper bounds. A similar trend is observed in the comparison to amide NOEs

(Fig. S4) which shows overall good agreement but with a few NOEs violating at similar positions as for the methyl NOEs.

As a final consistency check, we also compared the simulations to the SANS data for ΔH5-DMPC. The scattering contrast is very different in SAXS and SANS, and the scattering from the lipid bilayer has a relatively higher amplitude in the latter. This gives an independent check that the simulation provides a good description of the structure of the lipid bilayer. As the SEC-SANS data were measured on a His-tagged ΔH5-DMPC nanodisc, we therefore simulated this situation by creating an ensemble of His-tag structures and randomly sampled and attached these to the outer MSP-belts in the simulation frames under the assumption that the His-tags are disordered on the nanodiscs (Fig. S5). As for the SAXS and NOE data we also here find a generally good agreement.

Integrating experiments and simulations

While the MD simulations are generally in very good agreement with the SAXS and NMR data, there remain discrepancies that could contain information about the conformational ensemble of ΔH5-DMPC in solution. We therefore used a previously described Bayesian/Maximum Entropy (BME) approach[16–19,31] to integrate the MD simulations with the SAXS and NMR data. Briefly, the BME method refines the simulation against measured experimental averages by adjusting the weights of each frame in the simulation. To do so, BME finds the optimal balance between 1) minimizing the discrepancy between the simulation and the observed experimental averages and 2) ensuring as little perturbation of the original simulation as possible thereby limiting chances of overfitting. The outcome is a conformational ensemble that is more likely to represent ΔH5-DMPC in solution. In practice, this is achieved by changing the weight of each configuration in the ensemble obtained from the MD simulations, and we therefore call this a 'reweighted ensemble'.[19,32] The amount of reweighting can be quantified by an entropy change (S_{rel}) that reports on how much the weights had to be changed to fit the data[18,19] (see Methods). Alternatively, the value $N_{eff} = \exp(S_{rel})$ reports

on the effective ensemble size, that is what fraction of the original frames that were used to derive the final ensemble.

We used both the SAXS and NOE data individually, as well as combined, to understand the effects of each source of data on the reweighted conformational ensemble (Table 2). We note that when a specific type of data is used to generate the ensemble, the resulting χ^2 simply reports on how well the simulation has been fitted to the data; because of the maximum-entropy regularization to avoid overfitting, we do not fit the data as accurately as possible. The two types of experimental data complement each other in structural information content. Specifically, the SAXS data report on the overall size and shape, and is sensitive to both the protein and the lipids through atom-atom pair distributions in a range from 10 Å to 1000 Å, whereas the NOEs contain local, specific atom-atom distances from the protein belts of the ΔH5 but not any direct information about the lipids.

We find that refining the simulations against the SAXS data primarily improves the agreement with that data, but does not substantially improve agreement with the NOEs. A similar observation was made when refining against the NMR data. Thus, the two data types only improve the MD trajectory with respect to the structural properties they are sensitive to, but do not compensate for other structural inaccuracies in the simulation, again highlighting the orthogonal information in the two sources of information. In addition, we performed reweighting with the methyl NOEs and the amide NOEs separately (Table S1). The already low discrepancy of the amide NOEs barely improves while the discrepancies of both methyl NOEs and SAXS are unaffected by integration with amide NOEs alone, implying that the structural information content contained in the amide NOEs is already correctly captured by the force field. Thus, as expected, reweighting against a source of data where there is already good agreement has little effect on the conformational ensemble.

Because the NOE and SAXS experiments provide independent information we refined the ensemble against both sets of data (Fig. 4). We find that we can fit both sources of data at reasonable accuracy without dramatic changes of the weights away from the

Boltzmann distribution of the force field ($N_{\text{eff}} = 18\%$). We thus proceed with our analysis of the structural features of ΔH5-DMPC using an ensemble of conformations that is based on integrating the MD simulations with both the SAXS and NOE experiments. For comparison we also present the structural features based only on the MD simulation trajectory i.e. before reweighting the simulation against experiments.

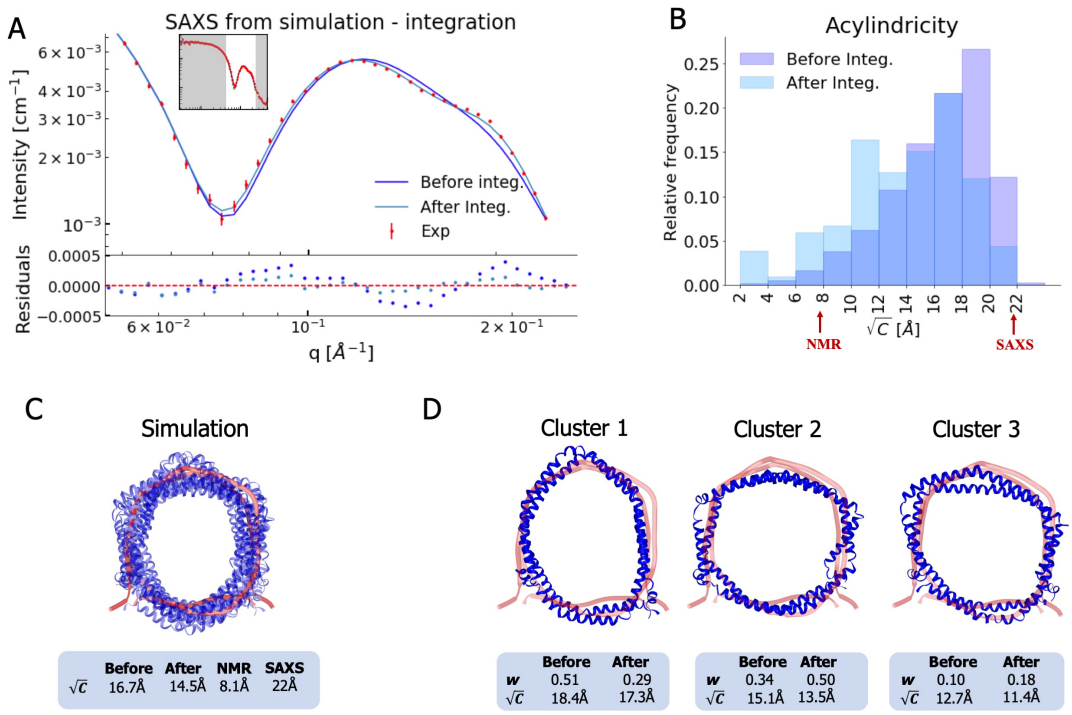

Figure 4: ***Integrating simulations and experiments.*** ***A)*** *SAXS data calculated from the simulation before and after reweighting the ensemble using experimental data. Only the high q-range is shown as the discrepancy between simulation and experiments are mainly located here, for the entire q-range see Fig. S6. Agreement with the NOEs before and after integration are likewise shown in Fig. S7.* ***B)****. Histogram of the acylindricity of the simulations ($\sqrt{C}$) both before integration (dark blue) and after integration (light blue).* ***C)*** *Visualization of the conformational ensemble showing structures sampled every 100 ns in cartoon representation (blue), the original NMR/EPR structure is shown in rope representation for comparison (red). The table below shows the acylindricity of the entire conformational ensemble before and after integration and compared to the original NMR/EPR (NMR) structure and the SAXS/SANS model fit.* ***D)*** *Weights and acylindricity of the three main clusters of the MD simulation (blue) before and after integration.*

Analysis of the measured SAXS and SANS revealed an elliptical shape of the ΔH5-DMPC upon fitting of a single structure to the data, i.e. an time- and ensemble averaged structure. In contrast, the previously integrative NMR/EPR method gave rise to a more circular configuration upon fitting a single structure. Combining the results of the two studies, we hypothesized that the nanodisc possesses underlying elliptical fluctuations with the major axis changing within the nanodisc. In such a system NMR and EPR measurements, which build on ensemble averaged information of specific atom-atom interactions, will give rise to an on-average circular structure. SAXS and SANS, on the contrary, which build on distributions of global distances rather than specific atom-atom distances, will not distinguish between the orientation of the major axis within the nanodisc and thus give rise to observations of an elliptical shape. By complementing the experiments with MD simulations we obtained a trajectory with structural features that supports this hypothesis.

To investigate the hypothesis further, we quantified the degree of ellipticity in terms of an acylindricity parameter, C, defined as the difference between the x and y components of the gyration tensor (see Methods for details). C is thus a measure of how far from a perfect circular cylinder the shape is, and $C = 0$ corresponds to a circular cylinder. We calculated both the average and distribution of the acylindricity from the simulated ensemble both before and after reweighting against the experimental data (Fig. 4B and 4C). In addition, we calculated the acylindricity of both the integrative NMR structure and from the structural model obtained from the SAXS and SANS measurements.

We find that the acylindricity decreased from $\sqrt{C} = 17$ Å in the original MD simulation trajectory to $\sqrt{C} = 15$ Å after integration of the NMR and SAXS data, showing that the experiments indeed affect the structural features and is of importance. This value and that obtained from the analytical geometric model fitted to the SAXS data ($\sqrt{C} = 22$ Å), are both somewhat higher than that of the integrative integrative NMR/EPR structure ($\sqrt{C} = 8.1$ Å) reported by Bibow *et al.*[14] Thus, the acylindricity of the final, heterogenous ensemble (15 Å) lies between that of the two conformations that were fitted individually to either the NMR

(8 Å) or SAXS data (22 Å).

To understand the elliptical shape of the ΔH5-DMPC nanodisc better and the role played by reweighting against experiments, we calculated the average acylindricity for each cluster of conformations of ΔH5-DMPC both before and after integration with experimental data (Fig. 4D). We note that because our reweighting procedure acts on the individual conformations and not at the coarser level of clusters, the average acylindricity changes slightly for each cluster upon reweighting. Clusters 1 and 2, which together constitute about 80% of the conformational ensemble (both before and after reweighting), are both clusters with high acylindricity, but with orthogonal directions of the major axis in the elliptical structure. The major change after integration is the exchange in populations of the two clusters resulting in cluster 2 to be weighted highest underlining the influence and importance of the integration. Thus, our MD simulations and the integration with the experiments support the hypothesis of underlying elliptical fluctuations with the major axis changing direction inside the nanodisc, and we note that the detailed molecular description of this was only possible by combining the MD simulations with both the SAXS and NMR data.

Conclusions

Lipid nanodiscs are versatile membrane mimetics with a wide potential for studies of the structure, function and dynamics of membrane proteins. Despite their widespread use and numerous studies, we still do not have a full and detailed understanding of the structural and dynamic features of nanodiscs. This in turn limits our ability to interpret e.g. solution scattering experiments when membrane proteins are embedded into such nanodiscs. In order to further our understanding of the conformations and structural fluctuations of both the protein and lipid components in nanodiscs, we have performed a series of biophysical experiments on DMPC-loaded ΔH5 and ΔH4H5 nanodiscs. We used DSC to investigate the lipid melting transition in the small nanodiscs in comparison to the more biological lipid vesicles

by DSC and found that the melting takes place over a much broader temperature range in the small nanodiscs. The observed correlation between the size of the belt proteins and the lipid melting enthalpy give support to the proposition,[21] that the arrangement of the lipids near the nanodisc rim must be highly perturbed. Using SEC-SAXS and SEC-SANS measurements, we investigated the solution structure of the ΔH4H5-DMPC and ΔH5-DMPC. Model-based analysis of this data showed an 'average' elliptical shape of both nanodiscs. In contrast, a previously determined integrative NMR/EPR[14] method gave rise to a more circular average structure of the ΔH5 nanodisc. We reconcile these two apparently opposing views and provide a richer and more detailed view of the nanodisc and its dynamics by performing MD simulations. In particular, we used a Bayesian/Maximum Entropy approach to integrate the MD simulations with the SAXS and NMR data to uncovering the existence of underlying fluctuations between elliptical shapes with orthogonal major axes in consistency with both sources of data. We note that the NMR/EPR-derived structure, and our MD simulations initiated from this structure, provide very good agreement with the SAXS data even without reweighting. Because our SAXS data are rather precise, however, we were able to detect subtle deviations that enabled us to refine our model. Thus, we stress that approaches such as the one described here takes advantage of the increasing possibilities for accurate NMR and scattering data in solution, strongly improved models for lipid bilayers for certain lipid types as well as new approaches to integrate experiments and simulations. In this way, our study exemplifies how integrating multiple biophysical experiments and simulations may lead to new insight into a complex system and paves the way for future studies of membrane proteins.

Methods

Expression

The constructs for ΔH4H5 and ΔH5 are those reported by Hagn et al.[3]. The expression was performed according to established procedures[20] while the purification protocol was slightly modified from the published version.[20] The cells were opened in lysis buffer containing 50 mM Tris/HCl pH 8.0, 300 mM NaCl, 1% Triton X-100 and 6 M GuHCl by vigorous shaking for 15 min. Insoluble material was subsequently removed by centrifugation at 18,000 rpm for 1 hour using an SS-34 rotor. The supernatant was loaded on Ni-NTA resin pre-equilibrated in lysis buffer and washed extensively with the same buffer. Extensive washes using lysis buffer without GuHCl and subsequently wash buffer containing 50 mM Tris/HCl pH 8.0, 300 mM NaCl, 20 mM Imidazole and 50 mM Cholate was performed in order to remove GuHCl and Triton X-100. Protein was eluded in buffer containing 50 mM Tris/HCl pH 8.0, 300 mM NaCl, 500 mM Imidazole, concentrated, flash frozen and stored at -80 °C until further use. For constructs without His-TEV tags, the cleavage of the TEV-site was performed by adding DDT and TEV protease to a final concentration of 1 mM and 1:20 respectively and incubated at room temperature for 6-12 hours. Any un-cleaved MSP and TEV protease was removed by passing the solution over Ni-NTA resin again.

Assembly of Nanodiscs

Before assembly, the DMPC lipids were suspended in a buffer containing 100 mM NaCl, 20 mM Tris/HCl pH 7.5, and 100 mM sodium cholate detergent to a final lipid concentration of 50 mM. All lipids used were obtained from Avanti Polar Lipids.[33]

The lipid and MSP stock solutions were mixed with the selected molar concentration ratios in the range from 1:9 to 1:80 depening on the sample (see e.g. S1). Cholate was removed after mixing by addition of an excess amount of Amberlite detergent absorbing beads to start the assembly of the nanodiscs. The samples were left in a thermomixer

for 4 hours at 28 °C. The Amberlite was then removed by spinning the solution down at 5000 rpm. Purification was performed using size exclusion chromatography on an Äkta purifier (HPLC) system with a Superdex200 10/300 column from GE Healthcare Life Science (S200).[34]

Differential Scanning Calorimetry (DSC)

The measurements were performed on a VP-DSC (MicroCal) using a constant pressure of 1.7 bar (25 psi) and a scan rate of 1 °C/min between 6 °C and 40 °C. All samples had been purified in PBS buffer prior to the measurement. Data was background subtracted and baseline corrected in the Origin instrument software using a "Cubic Connect" baseline correction. Finally, the data was normalized by the lipid concentration of the individual samples.

SEC-SANS

SEC-SANS was performed at the D22 small-angle scattering diffractometer at the ILL, Grenoble, France using a very recently developed SEC-SANS setup.[35,36] Briefly, the setup was as follows: the *in situ* SEC was done using a modular HPLC system (Serlabo) equipped with a Superdex200 10/300 GL gel filtration column (GE) with a void volume of approximately 7.5 ml and a flow rate of 0.25 ml/min. The SmartLine 2600 diode-array spectrophotometer (Knauer) was connected via optic fibers either to an optic cell of 3 mm path length placed at the outlet of the chromatography column, enabling the simultaneous recording of chromatograms at four different wavelengths, including 280 nm which we used for the concentration determination.

All components of the HPLC setup including buffers and the column were placed in a closed cabinet connected to an air-cooling system set to 10 °C to control the temperature of the sample. Before measurements, we equilibrated the column in a D_2O-based buffer, and the buffer in the sample was exchanged to a D_2O-based buffer using a illustra NAP-25

gravity flow column (GE).[34] The D_2O buffer contained 20 mM TrisDCl pH 7.5 and 100 mM NaCl.

The experiments were carried out with a nominal neutron wavelength, λ, of 6.0 Å and a wavelength distribution, $\Delta\lambda/\lambda = 10\%$ FWHM, a rectangular collimation of 40 mm × 55 mm and a rectangular sample aperture of 7 mm × 10 mm. The distance of the sample-detector used for the characterization of the empty nanodiscs was 5.6 m (with collimation of 5.6 m), covering a momentum transfer range, q, of 0.0087 Å^{-1} to 0.17 Å^{-1}, with $q = 4\pi \sin(\theta)/\lambda$, where θ is half the angle between the incoming and the scattered neutrons. Measured intensities were binned into 30 s frames. Sample transmission was approximated by the buffer measured at the sample-detector distance of 11.2 m. The measured intensity was brought to absolute scale in units of scattering cross section per unit volume (cm^{-1}) using direct beam flux measured for each collimation prior to the experiment. Data reduction was performed using the GRASP software.[37] The SANS data appropriate for buffer subtraction was identified based on when the 280 nm absorption during the SEC curve showed no trace of protein.

SEC-SAXS

SEC-SAXS was performed at the BioSAXS instrument at BM29 at the ESRF, Grenoble, France.[38] Briefly, the setup at BM29 included an HPLC controlled separately from the SAXS measurement, coupled to a UV-Vis array spectrophotometer collecting absorption from 190 nm to 800 nm. Data were collected with a wavelength of 0.9919 Å using a sample-detector distance of 2.87 m which provided scattering momentum transfers ranging from 0.003 Å^{-1} to 0.49 Å^{-1}. The capillary was cooled to 10 °C, however, the HPLC including the SEC-column was placed at ambient temperature. Size exclusion chromatography was performed using the exact same column as for SEC-SANS and equivalent H_2O-based buffer. A flow rate of 0.5 ml/min was used. Data reduction was carried out using the in-house software, and subsequent conversion to absolute units was done with water as calibration

standard.[39] The 1 s frames recorded were subsequently averaged in 10 s bins.

Standard solution SAXS

Standard solution SAXS data were obtained at the P12 beamline at the PETRA III storage ring in Hamburg, Germany[40] using a wavelength of 1.24 Å, a sample-detector distance of 3 m, providing a momentum transfers covering from 0.0026 $Å^{-1}$ to 0.498 $Å^{-1}$ and a variable temperature in the exposure unit. 20 exposures of 0.045 seconds were averaged, background subtracted and normalized by the available software at the beamline. The measurements were performed at both 10 °C and 30 °C.

SAXS and SANS data analysis.

The output of the SAXS and SANS experiments were small-angle scattering data in terms of absolute intensities $I(q)$. As usual, the scattering vector $q = 4\pi \sin\theta/\lambda$ where θ is the scattering angle and λ is the wavelength of the incoming beam. $I(q)$ was transformed into the pair distance distribution function, $p(r)$, by indirect Fourier transformations (IFT) which was performed at the BayesApp-server.[41]

SAXS/SANS modeling was carried out using our previously developed WillItFit software[23] which is available for download `https://sourceforge.net/projects/willitfit/`. The applied structural models (see futher description below) are an adaptation of similar models previously developed to analyse SAXS and SANS data from MSP1D1 nanodiscs.[6,22]

In brief, the model describes the nanodiscs of a certain ellipticity based on analytical form factors[42] as explained by Skar-Gislinge *et al.*[6,22] The ellipticity, in terms of the axis ratio is allowed to vary in the fit and can also take the size of unity corresponding to a circular disc. The model is fitted on absolute scale and utilizes information from the molecular composition of the applied protein belt and DMPC hydrophilic head and hydrophobic tail groups, provided via an input card to calculate the excess scattering length densities and total partial volumes of these compounds. Apart from the parameters listed in Table 1,

the model also fits a small constant background added to the model, and includes a term accounting for interface roughness, fixed to 2 Å in the present analysis, and where relevant, a Gaussian random coil description of the linked TEV-His-tag with $R_G = 12.7$ Å consistent with the assumption that the 23 amino acids of the tag are in a fully disordered state.[25]

MD simulations

The MD simulations were started from the first model in PDB ID 2N5E.[14] A total of 50 pre-equilibrated DMPC lipids[43,44] were inserted into each bilayer inside the protein belt. The number of lipids was chosen from the measured optimal reconstitution ratio, and in accordance with the reconstitution ratio used in the experiments for the NMR structure[14] as well as obtained from our fit of the geometric model to the SAXS and SANS data. The MD simulations were performed using the GROMACS 5.0.7 software package[45,46] and the CHARMM36m force field.[27] The system was solvated in a cubic box and neutralized by addition of Na^+ counter ions followed by a minimization of the solvent. Equilibration was performed in 6 steps following the protocol from CHARMM-GUI[47] with slow decrease in the positional restraint forces on both lipids and protein. The volume of the box was then equilibrated in the NPT ensemble at 303.15 K and 1 bar giving a final box with side lengths 13.2 nm. The production run was performed in the NVT ensemble at 303.15 K (above the phase transition of the DMPC lipids) using the stochastic velocity rescaling thermostat,[48] 2 fs time steps and the LINCS algorithm to constrain all bonds. We performed two production runs (lengths 600 ns and 595 ns) starting from the same equilibrated structure. We concatenated these two MD simulations into a single trajectory, which then represents our sample of the dynamics of the system. We clustered the conformations from the simulations (one structure extracted for every nanosecond) with the RMSD based Quality Threshold method[49,50] using C_α atoms only and with a cluster diameter cutoff of 0.58 nm; this resulted in six clusters.

Calculating SAXS and SANS from simulations

We performed SAXS calculations using both CRYSOL[30] and FOXS[28,29] on structures extracted every 1 ns from the simulations using fixed parameters and q-range from 0.0 Å^{-1} to 0.25 Å^{-1}. Most of the the overall structural information is contained within this q-range, and the calculations of SAXS intensities from the structures are also less accurate in the wide-angle regime. The SAXS profile of the NMR/EPR structure was calculated by adding DMPC lipids to the first model of the PDB entry and subsequent equilibration by MD (fixing the protein), and then using FOXS to back-calculate the SAXS. SANS calculations were performed using CRYSON[51] with the fraction of D_2O in solution set to 1.0 in accordance with the experimental measurements.

We used standard solution SAXS data experimental recorded at 30 °C on the ΔH5-DMPC (without His-TEV-tags) to compare to our simulations, as this setup is most similar to that used to derive the NMR/EPR structure. For more details on the SAXS/SANS calculations, see Supporting Information Text.

NOE calculations from simulations

We calculated distances corresponding to the experimentally observed NOEs on structures extracted every 1 ns from the simulations. To compare with the experimental distances, available as upper bounds, we averaged the distances, R, between the respective atoms (or the geometric center for pseudo atoms) as $\langle R^{-3}\rangle^{-1/3}$.[52] When calculating χ^2 for validation we only include those distances where this average exceeded the experimentally-determined upper-bounds.

Integrating experiments and simulations

We used a Bayesian/maximum entropy approach,[16–18] as implemented in the BME software[19] (`github.com/KULL-Centre/BME`), to integrate the molecular simulations with the SAXS and

NMR experiments. The name originates from the two equivalent approaches, Bayesian and Maximum Entropy ensemble refinement, which are equivalent when the errors are modelled as Gaussians.[16,19,31] We here provide a brief overview of the approach and refer the reader to recent papers for more details.[16,19,31]

Given that our MD simulations provide a good, but non-perfect, agreement with experiments the goal is to find an improved description of the nanodisc that simultaneously satisfies two criteria: (i) the new ensemble should match the data better than the original MD ensemble and (ii) the new ensemble should be a minimal perturbation of that obtained in our simulations with the CHARMM36m force field in accordance with the maximum entropy principle. In a Bayesian formulation, the MD simulation is treated as a *prior* distribution and we seek a *posterior* that improves agreement with experiments. This may be achieved by changing the weight, w_j, of each conformation in the MD-derived ensemble by minimizing the negative log-likelihood function:[16,19]

$$\mathcal{L}(w_1 \dots w_n) = \frac{m}{2}\chi_r^2(w_1 \dots w_n) - \theta S_{\text{rel}}(w_1 \dots w_n). \tag{1}$$

Here, the reduced χ_r^2 quantifies the agreement between the experimental data (F_i^{EXP}) and the corresponding ensemble values, ($F(\mathbf{x})$), calculated from the weighted conformers ($\mathbf{x}$):

$$\chi_r^2(w_1 \dots w_n) = \frac{1}{m}\sum_i^m \frac{(\sum_j^n w_j F_i(\mathbf{x}_j) - F_i^{EXP})^2}{\sigma_i^2}. \tag{2}$$

The second term contains the relative entropy, S_{rel}, which measures the deviation between the original ensemble (with initial weights w_j^0 that are uniform in the case of a standard MD simulation) and the reweighted ensemble $S_{\text{rel}} = -\sum_j^n w_j \log\left(\frac{w_j}{w_j^0}\right)$. The temperature-like parameter θ tunes the balance between fitting the data accurately (low χ_r^2) and not deviating too much from the prior (low S_{rel}). It is a hyperparameter that needs to be determined (Fig. S8). In practice it turns out that minimizing $\mathcal{L}$ can be done efficiently by finding Lagrange multipliers in an equivalent Maximum Entropy formalism and we refer the

reader to previous papers for a full description and discussion of the approaches including how to determine θ.[16,19,31]

Acylindricity

In order to quantify how 'elliptical' the different nanodisc conformations are, we calculated the square root of the acylindricity, $\sqrt{C}$, where the acylindricity is defined from the principal components of the gyration tensor as $C := \lambda_x^2 - \lambda_y^2$, where the z-axis is orthogonal to the membrane and has the smallest principal component. In our calculations we included only the protein backbone atoms (excluding also the flexible tails from residues 55-63). This choice also makes it possible to compare with a similar calculation from the geometric model fitted from the SAXS and SANS data where the acylindricity was calculated using the major and minor axes from the geometric fit.

Acknowledgements

The research described here was supported by a grant from the Lundbeck Foundation to the BRAINSTRUC structural biology initiative, a Hallas-Møller Stipend from the Novo Nordisk Foundation and a grant from the Velux Foundations.

References

(1) Bayburt, T. H.; Grinkova, Y. V.; Sligar, S. G. *Nano Letters* **2002**, *2*, 853–856.

(2) Denisov, I. G.; Grinkova, Y. V.; Lazarides, A. A.; Sligar, S. G. *Journal of the American Chemical Society* **2004**, *126*, 3477–3487.

(3) Hagn, F.; Etzkorn, M.; Raschle, T.; Wagner, G. *Journal of the American Chemical Society* **2013**, *135*, 1919–1925.

(4) Marty, M. T.; Zhang, H.; Cui, W.; Gross, M. L.; Sligar, S. G. *Journal of The American Society for Mass Spectrometry* **2014**, *25*, 269–277.

(5) Marty, M. T.; Baldwin, A. J.; Marklund, E. G.; Hochberg, G. K. A.; Benesch, J. L. P.; Robinson, C. V. *Analytical Chemistry* **2015**, *87*, 4370–4376.

(6) Skar-Gislinge, N.; Simonsen, J. B.; Mortensen, K.; Feidenhansl, R.; Sligar, S. G.; Lindberg Mller, B.; Bjrnholm, T.; Arleth, L. *Journal of the American Chemical Society* **2010**, *132*, 13713–13722.

(7) Midtgaard, S. R.; Pedersen, M. C.; Kirkensgaard, J. J. K.; Sorensen, K. K.; Mortensen, K.; Jensen, K. J.; Arleth, L. *Soft Matter* **2014**, *10*, 738–752.

(8) Midtgaard, S.; Pedersen, M.; Arleth, L. *Biophysical Journal* **2015**, *109*, 308–318.

(9) Shih, A. Y.; Denisov, I. G.; Phillips, J. C.; Sligar, S. G.; Schulten, K. *Biophysical Journal* **2005**, *88*, 548–556.

(10) Shih, A. Y.; Arkhipov, A.; Freddolino, P. L.; Sligar, S. G.; Schulten, K. *Journal of Physical Chemistry B* **2007**, *111*, 11095–11104.

(11) Siuda, I.; Tieleman, D. P. *Journal of Chemical Theory and Computation* **2015**, *11*, 4923–4932.

(12) Debnath, A.; Schäfer, L. V. *Journal of Physical Chemistry B* **2015**, *119*, 6991–7002.

(13) Vestergaard, M.; Kraft, J. F.; Vosegaard, T.; Thøgersen, L.; Schiøtt, B. *Journal of Physical Chemistry B* **2015**, *119*, 15831–15843.

(14) Bibow, S.; Polyhach, Y.; Eichmann, C.; Chi, C. N.; Kowal, J.; Albiez, S.; McLeod, R. A.; Stahlberg, H.; Jeschke, G.; Güntert, P.; Riek, R. *Nature Structural and Molecular Biology* **2017**, *24*, 187–193.

(15) Martinez, D.; Decossas, M.; Kowal, J.; Frey, L.; Stahlberg, H.; Dufourc, E. J.; Riek, R.; Habenstein, B.; Bibow, S.; Loquet, A. *ChemPhysChem* **2017**, *18*, 2651–2657.

(16) Hummer, G.; Köfinger, J. *Journal of Chemical Physics* **2015**, *143*, 243150.

(17) Róycki, B.; Kim, Y. C.; Hummer, G. *Structure* **2011**, *19*, 109–116.

(18) Bottaro, S.; Bussi, G.; Kennedy, S. D.; Turner, D. H.; Lindorff-Larsen, K. *Science Advances* **2018**, *4*, eaar8521.

(19) Bottaro, S.; Bengtsen, T.; Lindorff-Larsen, K. *bioRxiv* **2018**, 457952.

(20) Ritchie, T. K.; Grinkova, Y. V.; Bayburt, T. H.; Denisov, I. G.; Zolnerciks, J. K.; Atkins, W. M.; Sligar, S. G. *Methods in Enzymology*; Elsevier Masson SAS, 2009; Vol. 464; pp 211–231.

(21) Denisov, I. G.; McLean, M. A.; Shaw, A. W.; Grinkova, Y. V.; Sligar, S. G. *The Journal of Physical Chemistry B* **2005**, *109*, 15580–15588.

(22) Skar-Gislinge, N.; Arleth, L. *Physical Chemistry Chemical Physics* **2011**, *13*, 3161–3170.

(23) Pedersen, M. C.; Arleth, L.; Mortensen, K. *Journal of Applied Crystallography* **2013**, *46*, 1894–1898.

(24) Tristram-Nagle, S.; Liu, Y.; Legleiter, J.; Nagle, J. F. *Biophysical journal* **2002**, *83*, 3324–3335.

(25) Kohn, J. E.; Millett, I. S.; Jacob, J.; Zagrovic, B.; Dillon, T. M.; Cingel, N.; Dothager, R. S.; Seifert, S.; Thiyagarajan, P.; Sosnick, T. R.; Hasan, M. Z.; Pande, V. S.; Ruczinski, I.; Doniach, S.; Plaxco, K. W. *Proceedings of the National Academy of Sciences* **2004**, *101*, 12491–12496.

(26) Graziano, V.; Miller, L.; Yang, L. *Journal of Applied Crystallography* **2018**, *51*, 157–166.

(27) Huang, J.; Rauscher, S.; Nawrocki, G.; Ran, T.; Feig, M.; De Groot, B. L.; Grubmüller, H.; MacKerell, A. D. *Nature Methods* **2016**, *14*, 71–73.

(28) Schneidman-Duhovny, D.; Hammel, M.; Tainer, J. A.; Sali, A. *Biophysical Journal* **2013**, *105*, 962–974.

(29) Schneidman-Duhovny, D.; Hammel, M.; Tainer, J. A.; Sali, A. *Nucleic Acids Research* **2016**, *44*, W424–W429.

(30) Svergun, D.; Barberato, C.; Koch, M. H. *Journal of Applied Crystallography* **1995**, *28*, 768–773.

(31) Cesari, A.; Gil-Ley, A.; Bussi, G. *Journal of Chemical Theory and Computation* **2016**, *12*, 6192–6200.

(32) Bottaro, S.; Lindorff-Larsen, K. *Science* **2018**, *361*, 355–360.

(33) Avanti Lipids Polar Inc, 1,2-dimyristoyl-sn-glycero-3-phosphocholine. `https://avantilipids.com/product/850345`, 2018; [accessed 23 Sep. 2018].

(34) GE Healthcare Life Sciences, Superdex 200 10/300 GL and 5/150 GL. `https://www.gelifesciences.com/en/in/shop/chromatography/prepacked-columns/`

size-exclusion/superdex-200-10-300-gl-and-5-150-gl-p-05902, 2018; [accessed 23 Sep. 2018].

(35) Jordan, A.; Jacques, M.; Merrick, C.; Devos, J.; Forsyth, V. T.; Porcar, L.; Martel, A. *Journal of Applied Crystallography* **2016**, *49*, 2015–2020.

(36) Johansen, N. T.; Pedersen, M. C.; Porcar, L.; Martel, A.; Arleth, L. *Acta Crystallographica Section D Structural Biology* **2018**, *74*, 1178–1191.

(37) Lise, A.; Holm, V. L.; Nicolai, J.; Andreas, L.; Anne, M.; Soren, M.; Lionel, P.; Nicholas, S.-G. SEC-SANS for probing the structure of membrane proteins in lipid-protein nanodiscs. 2016.

(38) Pernot, P. et al. *Journal of Synchrotron Radiation* **2013**, *20*, 660–664.

(39) Orthaber, D.; Bergmann, A.; Glatter, O. *Journal of Applied Crystallography* **2000**, *33*, 218–225.

(40) Blanchet, C. E.; Spilotros, A.; Schwemmer, F.; Graewert, M. A.; Kikhney, A.; Jeffries, C. M.; Franke, D.; Mark, D.; Zengerle, R.; Cipriani, F.; Fiedler, S.; Roessle, M.; Svergun, D. I. *Journal of Applied Crystallography* **2015**, *48*, 431–443.

(41) Hansen, S. *Journal of Applied Crystallography* **2014**, *47*, 1469–1471.

(42) Pedersen, J. S. *Advances in Colloid and Interface Science* **1997**, *70*, 171–210.

(43) Domański, J.; Stansfeld, P. J.; Sansom, M. S. P.; Beckstein, O. *Journal of Membrane Biology* **2010**, *236*, 255–258.

(44) Dickson, C. J.; Rosso, L.; Betz, R. M.; Walker, R. C.; Gould, I. R. *Soft Matter* **2012**, *8*, 9617.

(45) Pronk, S.; Páll, S.; Schulz, R.; Larsson, P.; Bjelkmar, P.; Apostolov, R.; Shirts, M. R.; Smith, J. C.; Kasson, P. M.; Van Der Spoel, D.; Hess, B.; Lindahl, E. *Bioinformatics* **2013**, *29*, 845–854.

(46) Abraham, M. J.; Murtola, T.; Schulz, R.; Páll, S.; Smith, J. C.; Hess, B.; Lindah, E. *SoftwareX* **2015**, *1-2*, 19–25.

(47) Lee, J. et al. *Journal of Chemical Theory and Computation* **2016**, *12*, 405–413.

(48) Bussi, G.; Donadio, D.; Parrinello, M. *Journal of Chemical Physics* **2007**, *126*.

(49) Heyer, L. J.; Kruglyak, S.; Yooseph, S. *Genome research* **1999**, *9*, 1106–1115.

(50) Melvin, R. L.; Gmeiner, W. H.; Salsbury, F. R. *The journal of physical chemistry. B* **2016**, *120*, 10269–10279.

(51) Svergun, D. I.; Richard, S.; Koch, M. H.; Sayers, Z.; Kuprin, S.; Zaccai, G. *Proceedings of the National Academy of Sciences of the United States of America* **1998**, *95*, 2267–2272.

(52) Tropp, J. *The Journal of Chemical Physics* **1980**, *72*, 6035–6043.